Lab on a Chip

PAPER

View Article Online
View Journal | View Issue

Cite this: *Lab Chip*, 2016, **16**, 3804

Autonomous microfluidic capillaric circuits replicated from 3D-printed molds†

A. O. Olanrewaju,[ab] A. Robillard,[ab] M. Dagher[ab] and D. Juncker*[abc]

Received 15th June 2016,
Accepted 11th August 2016

DOI: 10.1039/c6lc00764c

www.rsc.org/loc

We recently developed capillaric circuits (CCs) – advanced capillary microfluidic devices assembled from capillary fluidic elements in a modular manner similar to the design of electric circuits (Safavieh & Juncker, *Lab Chip*, 2013, **13**, 4180–4189). CCs choreograph liquid delivery operations according to pre-programmed capillary pressure differences with minimal user intervention. CCs were thought to require high-precision micron-scale features manufactured by conventional photolithography, which is slow and expensive. Here we present CCs manufactured rapidly and inexpensively using 3D-printed molds. Molds for CCs were fabricated with a benchtop 3D-printer, poly(dimethylsiloxane) replicas were made, and fluidic functionality was verified with aqueous solutions. We established design rules for CCs by a combination of modelling and experimentation. The functionality and reliability of trigger valves – an essential fluidic element that stops one liquid until flow is triggered by a second liquid – was tested for different geometries and different solutions. Trigger valves with geometries up to 80-fold larger than cleanroom-fabricated ones were found to function reliably. We designed retention burst valves that encode sequential liquid delivery using capillary pressure differences encoded by systematically varied heights and widths. Using an electrical circuit analogue of the CC, we established design rules to ensure strictly sequential liquid delivery. CCs autonomously delivered eight liquids in a pre-determined sequence in <7 min. Taken together, our results demonstrate that 3D-printing lowers the bar for other researchers to access capillary microfluidic valves and CCs for autonomous liquid delivery with applications in diagnostics, research and education.

Introduction

Capillary-driven microfluidic devices move liquids using capillary forces defined by the geometry and surface chemistry of microchannels. This allows liquid delivery without using external pumps and valves. A wide range of capillary fluidic control elements were developed over the years including: stop valves,[1] retention valves,[2] trigger valves,[3] and capillary pumps.[2,4,5] Autonomous capillary microfluidic systems capable of self-powered and self-regulated completion of biochemical assays were also developed.[2,6–8] Yet these autonomous capillary microfluidic systems were fabricated using silicon wafers and cleanroom processes with multiple photomasks, thereby increasing their cost and complexity. Paper-based microfluidics and lateral flow assays were also rediscovered as inexpensive approaches to autonomous capillary-driven flow;[9,10] nevertheless, paper-based methods rely on heterogeneous porous substrates with statistical flow paths and cannot accomplish some of the valving capabilities that require the deterministic and predictable flow paths of microchannel-based devices. As such, there is a need for rapid and inexpensive fabrication of microchannel-based capillary microfluidics.

Capillaric circuits for autonomous liquid delivery

More recently, advanced capillary microfluidic devices capable of pre-programmed delivery of multiple liquids were developed to enable autonomous multi-step processes, for instance to incorporate wash or signal amplification steps for improved bioassay sensitivity and specificity.[11–13] Our research group proposed capillaric circuits (CCs) – advanced capillary circuits that are assembled from individual capillaric elements in the same way that electric circuits are assembled from individual electric components.[13] CCs operate in a walk-away format where the operator pre-loads each reservoir, without worrying about the timing or sequence of these operations – instead, capillary microfluidic elements choreograph liquid delivery operations with minimal user intervention. This makes CCs a desirable platform for automating

[a] *Biomedical Engineering Department, McGill University, 740 Dr Penfield Avenue, Montreal, QC, H3A 0G1, Canada. E-mail: david.juncker@mcgill.ca; Fax: +1 514 398 1790*
[b] *McGill University and Genome Quebec Innovation Centre, 740 Dr Penfield Avenue, Montreal, QC, H3A 0G1, Canada*
[c] *Department of Neurology and Neurosurgery, 740 Dr Penfield Avenue, Montreal, QC, H3A 0G1, Canada*

† Electronic supplementary information (ESI) available. See DOI: 10.1039/c6lc00764c

biochemical assays in point-of-care settings with minimal instrumentation.

The words *capillary* and *capillaric* are meant to emulate the distinction between *electric* and *electronic* whereas the former pertains to basic principles and the latter is used in the context of advanced circuits integrating multiple functionalities. In addition, the term *capillary* is ambiguous, as it is both used in reference to physical capillaries (including artificial and natural capillaries such as blood vessels) and in reference to surface tension-driven flow either within capillaries, microfluidic conduits or porous media, which can lead to confusion. The term *capillaric* is restricted to surface-tension driven microfluidic circuits, and thus helps resolve the ambiguity.

Our group introduced two new fluidic elements to enable deterministic flow control with CCs. First, we developed two-level trigger valves (TVs) that stop liquids for over 30 minutes using an abrupt geometry change and a hydrophobic PDMS cover, thereby enabling pre-loading of reservoirs and subsequent liquid release when flow is triggered by a connected channel.[13] We also developed retention burst valves (RBVs) that have a burst pressure encoded by their geometry. When integrated with other capillary fluidic elements within a CC, RBVs allow autonomous delivery of liquids in a pre-programmed sequence according to increasing order of RBV capillary pressure.[13]

Rapid prototyping of passive microfluidic devices

Although CCs enable sophisticated and automated fluidic operations, the prevailing view is that deterministic capillaric microfluidics require high-precision and small-scale ($\sim$10 μm) features for proper operation. As such, fabrication of CCs was dependent on cleanrooms, and was resource-intensive, time-consuming and expensive. Coupled with the need of photomasks for photolithography, a high cost and slow turnaround time for new design iterations limits the development of new devices and their widespread adoption.

To overcome the limitations of cleanroom fabrication, rapid and inexpensive prototyping of capillary microfluidic valves and integrated devices has been explored. Rapid prototyping techniques used for developing capillary microfluidic devices include micromilling[14] and laser cutting.[15] These techniques have successfully been used for making capillary stop valves using primarily hydrophobic surface coatings that greatly relax the design constraints on the valve, but at the expense of autonomy and thus require syringe pumps or centrifugal forces to move the liquids within the microchannels.[16–19] More recently, a simple, autonomous self-filling capillary system comprising a capillary TV was fabricated by CO_2 laser cutting.[15] These results suggested that larger scale capillary circuits may be possible, however the laser cutting created triangular shaped conduits with limited control over the channel dimension, thus preventing the integration of more advanced elements such as retention burst valves for making more advanced capillaric circuits.

3D-printed microfluidics

Lately, there has been a surge of interest in 3D-printing for microfluidics applications due to the speed, accessibility, and low cost required to fabricate multilayer microfluidic structures.

Recent reviews describe state of the art 3D-printing for microfluidics applications.[20,21] All demonstrations of 3D-printed microfluidics so far employ active flow control (usually pneumatic or centrifugal pumps). The resolution currently available with consumer grade 3D-printers is typically $\geq$200 μm (ref. 22, 23) with $\sim$1 μm surface roughness.[24] Capillary microfluidics however have traditionally been made with channels in the 1–100 μm range because the capillary pressure is inversely proportional to the smallest dimension, and becomes very small for large microchannels. Moreover, valving and flow control depend on the surface topography and abrupt geometric changes and low surface roughness are considered necessary to prevent pre-wetting and creeping flows. Hence the prevailing perception is that current 3D-printing technology may not be suitable for making capillary microfluidics because the smallest dimensions are too large to obtain adequate capillary pressure, the resolution and precision insufficient for making abrupt changes needed for reliable valves – notably due to the layered structure of stereolithographic printing forming steps that lend themselves to corner flow – and the high surface roughness may lead to creeping of liquid.

Capillaric circuits from 3D-printed molds

Here we present microfluidic capillaric circuits made from 3D-printed molds fabricated by stereolithographic 3D-printing with geometries scaled up >20-fold compared to cleanroom-fabricated circuits. 3D-printing allows rapid and inexpensive fabrication of CCs. This enables investigation and engineering of CCs with greater capabilities and increased accessibility in research and point-of-care settings. First, we 3D-print molds for TVs and characterize their performance as a function of geometry and surfactant concentration. Then we investigate design rules for CCs composed of TVs, RBVs, flow resistors, and capillary pumps using a proof of principle circuit with four reservoirs. Finally, we demonstrate the capabilities of our CCs by developing a circuit for autonomous delivery of eight liquids in <7 minutes.

Materials and methods

Process flow for 3D-printing capillaric circuits

First, we developed a symbolic representation for CCs using electrical analogies, as described in our previous work.[13] Next, the symbolic circuit was converted into a computer-aided schematic design that was exported into the standard stereolithography (STL) format for 3D-printing. We 3D-printed molds (negatives) of capillaric microfluidic devices using a stereolithography-based printer (Perfactory MicroEDU, EnvisionTEC Inc., Germany) with 96 μm *XY* pixel size and 50

μm *Z* layer height. Microfluidic features were aligned to the pixel grid of the 3D-printer projector to ensure accurate realization of features. The 3D-printer's default settings were used. Device designs included 2 mm thick bases for easier handling. The typical printing time for capillaric microfluidic devices, with multiple devices arranged to cover nearly the entire 100 × 75 mm^2 print area of the 3D-printer, was ~30 minutes. After 3D-printing, molds were washed in isopropanol for 5 minutes and dried with nitrogen gas. 3D-printed molds were inspected under the microscope to check for defects during the printing process.

PDMS replication from 3D-printed molds

To obtain multiple copies of capillary microfluidic devices from the same 3D-printed mold, we made poly(dimethylsiloxane) (PDMS) replicas of devices by soft lithography.[25] We 3D-printed molds using a high temperature molding resin (HTM140 resin, EnvisionTEC Inc., Germany) with a manufacturer-specified heat deflection temperature of 140 °C to allow replica molding of 3D-printed structures. Prior to PDMS replication, molds were pre-treated with a silicone spray (Ease Release 200®, Mann Formulated Products, USA) to prevent PDMS from sticking to the mold. The spray was applied in two passes uniformly over the surface of the mold from a height of about 10 cm. To make PDMS replicas, elastomer base and curing agent (Sylgard 184, Paisley Products Inc., Canada) were mixed in a 10 : 1 ratio. The PDMS mixture was degassed for 1 hour and poured onto the 3D-printed mold placed in a Petri dish. PDMS was cured overnight at 60 °C and then peeled from the mold. First PDMS replicas were discarded because they were sticky due to the presence of silicone spray residue; subsequent replicas were used for capillary microfluidics experiments.

Procedure for capillary-driven flow experiments

To obtain hydrophilic surfaces for capillary-driven flow, PDMS replicas were activated for 12 seconds at 200 mTorr and 150 W in a plasma chamber (PE-50, PlasmaEtch, USA). To characterize the plasma-treated surfaces, advancing and receding contact angles of deionized water were measured using a video-based optical contact angle measurement instrument (OCA 15EC, Dataphysics Instruments GmbH, Germany). Plasma-treated PDMS devices were sealed with flat, untreated PDMS covers to provide closed microchannels for capillary-driven flow. The PDMS covers were made with a 1 : 20 ratio of curing agent to elastomer base to obtain soft and flexible PDMS surfaces that sealed well, despite their hydrophobicity. Flow in CCs was tested using aqueous food dye solutions and visualized under a stereomicroscope (SMZ-8, Leica Microsystems Inc., Canada) with a video camera (Lumix GH3 DSLR, Panasonic Inc., Canada). During TV testing, when devices were tested for ≥30 min, we humidified the area around the capillary microfluidic chips with wet Kimwipes® and covered with a Petri dish to prevent evaporation.[26]

Results and discussion

CCs operate using a series of functional elements including inlets, channels, flow resistors, capillary pumps, trigger valves (TV), capillary retention valves, and retention burst valves (RBVs) that can be combined for encoding the autonomous delivery of multiple liquids.[13] The capillary pressure of each RBV is calculated using the Young–Laplace equation:

$$P = -\gamma\left(\frac{\cos\theta_t + \cos\theta_b}{h} + \frac{\cos\theta_r + \cos\theta_l}{w}\right) \quad (1)$$

where P is the capillary pressure, γ is the surface tension of liquid in the microchannel, and h, w, are the channel height and width respectively. θ_t, θ_b, θ_r, θ_l, are the top, bottom, right, and left channel wall contact angles, respectively. Contact angle hysteresis must be taken into account when designing RBVs since the advancing contact angles are relevant when a channel is filled while the receding contact angles are relevant when a channel is drained. Likewise, the resistance R for a conduit with a rectangular cross-section is given by:[27]

$$R = \frac{12\eta L}{\left[1 - 0.63(h/w)\right]}\frac{1}{\left(h^3 w\right)} \quad (2)$$

where η is the viscosity of liquid in the channel, and L is the length of the microchannel. The cross section of channels and various elements for microfabricated CCs reported by Safavieh *et al.*[13] ranged from 15 × 100 μm^2 to 200 × 200 μm^2. Thus, assuming receding contact angles of 89° and 31° for the hydrophobic top PDMS surface and hydrophilic side and bottom surfaces respectively, and a surface tension γ of 72 N m^{-1}, the capillary pressures of microchannels (calculated using eqn (1)) in the cleanroom-fabricated circuits ranged from −7948 Pa to −1264 Pa. These capillary pressures would correspond to water column heights of 810 mm and 129 mm respectively in capillary rise experiments. Since our microchannel lengths were on the order of 5 mm, capillary forces dominated gravity in our microfabricated CCs and our devices could be operated without considering gravity effects.

We first tested whether 3D-printed channels and capillary pumps replicated into PDMS could be filled by a liquid, and found that this worked reliably up to 1000 × 1000 μm^2 constituting the upper limit for capillary elements in this study. The lower size limit for fluidic elements was set by the resolution of the 3D printer. The vertical resolution was set by the thickness of each printed layer and was 50 μm. The lateral resolution was 100 μm under the best circumstances, but was limited to 200 μm when taking into consideration fabrication yield. Hence, for 3D-printed circuits, the cross-sectional dimensions range from 50 × 200 μm^2 to 1000 × 1000 μm^2, and the capillary pressure ranges from −955 Pa to −188 Pa, or a water column height from 97 mm to 19 mm. These type of conduits filled spontaneously with aqueous solutions and remain in a microfluidic regime where gravity and inertia within the conduits are negligible.

Next, we set out to test whether critical functional elements such as the TV and the RBV could also be 3D printed, whether surface roughness might affect their functionality, and to determine the design rules for making them.

Trigger valves

In order to develop functional CCs, the first step is to have functional and reliable trigger valves (TVs) to robustly hold liquids in reservoirs.[13] Consequently, we first characterized TVs on a standalone basis, before developing more complex CCs.

Cleanroom-fabricated *versus* 3D-printed trigger valves. Cleanroom fabrication is generally considered the gold standard for manufacturing capillary stop valves and TVs because of the small feature sizes and smooth channel surfaces attainable.[1,3,8,13,29] Cleanroom-fabricated TVs have small features (~20 μm) and smooth, vertical channel walls (Fig. 1a and c). Meanwhile, 3D-printed trigger features have larger minimum widths (≥100 μm) and rough, layered channel walls (Fig. 1b and d). These stark geometry differences call into question the functionality and reliability of 3D-printed TVs.

We 3D-printed TV molds and tested a wide range of geometries and surfactant concentrations to assess their functionality and reliability. Previously, the success rate of capillary stop valves and TVs was only reported over a 5 minute period.[15,28] Here we defined TV success as when a valve holds liquid for at least 30 minutes without leakage. This allowed autonomous microfluidic operations in a walk-away format where the user pre-loads samples and reagents onto the chip and subsequently starts the assay at a time of their choosing, without needing to fit their operations to a strict 5 minute window.

Effect of trigger valve geometry on success rate. The geometry of TVs influences their success rate.[18,28,29] Fig. 2a shows the geometric parameters known to affect the performance of capillary TVs: the height of the TV, width of the TV, and the height difference between the TV and its release channel. To determine which geometries provide high TV success rates, we tested valves with widths of 96 μm, 192 μm, 288 μm, 480 μm, 672 μm, 960 μm, and 2016 μm. TV heights were fixed at either 400 μm or 1000 μm to obtain different height-to-width ratios for these experiments. As summarized in Fig. 2b, all TVs tested were at least 75% successful (N = 8). The few failures were due to difficulties while loading valves with low (<1) or high (>5) aspect ratios (*i.e.* height-to-width ratios) that required the user to apply additional positive pressure when filling the valves. We found that 3D-printed TVs were reliable with dimensions up to 3 times larger than reported with CO_2 laser cutting[30] and up to 80 times larger than typical cleanroom-fabricated valves.[13,28]

Since the minimum z-layer thickness of the microchannels was limited to 50 μm by the 3D-printer resolution, we tested height differences of 100 μm, 150 μm, 200 μm, 250 μm, 300 μm, 400 μm, and 500 μm between the TV and the release channel. The TVs used for these height difference tests were 300 μm wide and 50 μm deep, since our TV characterizations showed reliable functionality over a wide range of geometries (Fig. 2b). As seen in Fig. 2c, the height difference between the TV and the release channel had a threshold effect on TV success. When the height difference was ≥300 μm, TVs were 100% successful (N = 6).

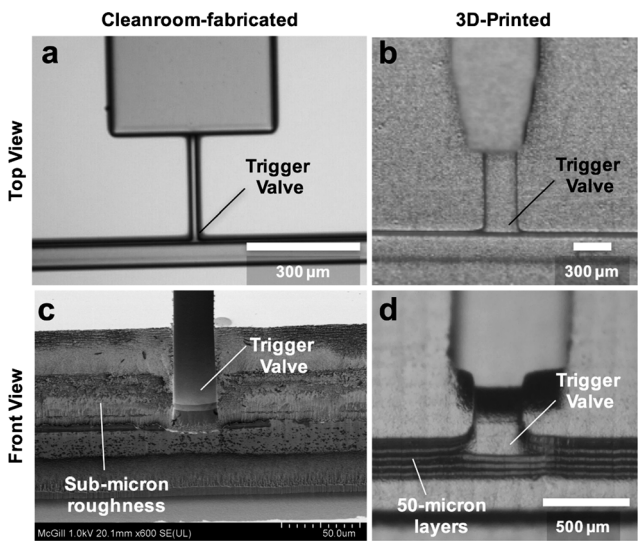

Fig. 1 Comparison between cleanroom-fabricated and 3D-printed TVs. a) Top view of TV fabricated by photolithography in the cleanroom showing smooth, high-precision features. b) Top view of TV fabricated by stereolithography-based 3D printing showing rough, large features. c) Scanning electron micrograph of TV fabricated by deep reactive ion etching of silicon showing vertical channel walls with sub-micron roughness. d) Front view of PDMS replica of 3D-printed TV showing 50 μm thick ridges on the channel wall due to the layer-by-layer printing process.

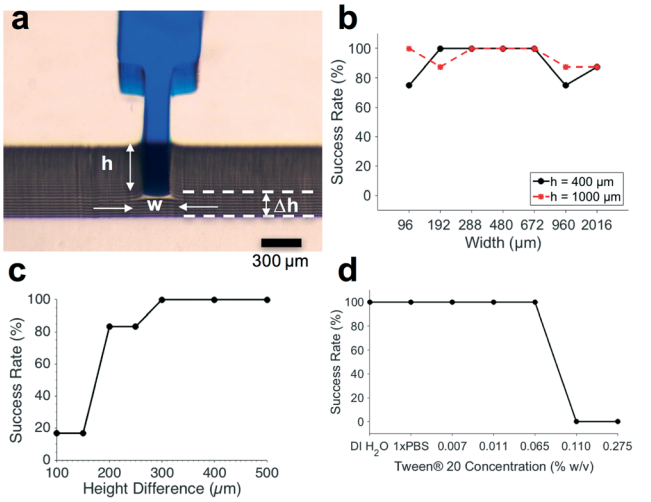

Fig. 2 Effect of geometry and surfactant concentration on success rate of TVs. a) Front view of food dye solution stopped at TV showing the TV height (h), width (w), and the height difference between TV and release channel (Δh). b) Success rates for TVs over a wide range of widths and heights. N = 8. c) Above a height difference (Δh) of 300 μm, TVs were 100% successful. N = 6. d) TVs were 100% successful at Tween® 20 concentrations ≤0.0650% weight/volume in 1 × PBS. N = 3.

Effect of surfactant concentration on trigger valve performance. Despite the fact that the most common application of capillary microfluidics is to automate biological assays that often require the use of surfactant-containing reagents, the effect of surfactant concentration on TV performance is not well reported in the literature. To determine the effect of surfactant on TVs, we tested aqueous solutions with different concentrations of Tween® 20, a surfactant commonly used in immunoassay wash buffers and for cell lysis. The critical micelle concentration of Tween® 20, is 0.0074% w/v. Consequently, we tested the following concentrations of Tween® 20: 0.0074, 0.0110, 0.0650, 0.1100, and 0.2750% weight/volume. As shown in Fig. 2d, we found that the TVs were 100% reliable when Tween® 20 concentrations were $\leq$0.0650% weight/volume (N = 3), a suitable surfactant concentration for use in wash buffers during immunoassays that commonly use 0.05%.[31,32]

Retention burst valves

Retention burst valves (RBVs) retain liquid in a conduit up to a threshold, or bursting, pressure which if exceeded leads to bursting of the valve and draining of the liquid held downstream in a reservoir. It is thus possible to drain a series of reservoirs connected to a main channel in a predetermined sequence by terminating each of them with a RBV with increasing burst pressure. The burst pressure of a RBV can be calculated using eqn (1) and using the receding contact angles for the liquid which were found to be 95° for the hydrophobic PDMS cover, and 31° for the hydrophilic bottom and side walls.

Capillaric circuit for autonomous delivery of four liquids. As a proof of principle that we could 3D-print molds for capillaric circuits, we designed a circuit with 4 RBVs (Fig. 3a and b). PDMS replicas of the 3D-printed mold were made (Fig. 3c), plasma-treated for hydrophilicity, and sealed with a hydrophobic PDMS cover (Fig. 3d). The expected pre-programmed operation of the CC is illustrated in Fig. 3e. First reservoirs were filled and TVs held each liquid in place. Next, a solution was added to the release channel, connecting the reservoirs to the pump and starting the pre-programmed liquid delivery sequence. Subsequently, the RBVs burst sequentially according to increasing capillary pressure.

The TVs in the CC were designed to have the smallest cross section in the circuit and the highest capillary pressure in the CC since they play a dual role – stopping liquids during initial filling of reservoirs, and acting as retention valves with higher capillary pressure than the capillary pump during reservoir drainage (see Fig. 3a). These retention valves ensure that the side branches are not completely emptied (with minimal dead volume), thereby allowing sequential liquid delivery without bubble trapping.[2,13]

In cleanroom-fabricated devices, multiple masks are needed for making structures with multiple depths; hence only the microchannel widths were used as a free parameter to adjust the RBV threshold.[13] RBVs were typically 100 μm deep and had widths of 200 μm, 130 μm, 110 μm, and 90 μm corresponding to capillary pressures of −1264 Pa, −1601 Pa, −1847 Pa, and −2028 Pa respectively.

With 3D-printing both the width and depth can be adjusted independently and fabricated in one shot. Consequently, we encoded the capillary pressure differences between RBVs by modifying both the height and widths of the microchannels. The lower size limit of our microchannels was set by 3D-printer resolution. The pixel size for the EnvisionTEC Perfactory MicroEDU 3D-printer is listed as 96 μm, the smallest features that we were able to print with a high yield were 200 μm wide and 50 μm deep open channels. This resolution obtained is similar to that reported for other state of the art stereolithographic 3D-printers in the literature.[20]

The reservoirs were 960 μm wide, 1000 μm deep, and 6250 μm long with a volume of 6 μL, corresponding to 60 times the volume of typical microfabricated reservoirs.[13] Due to the change in the size of the RBV, there were minor changes in volume for each reservoir (Fig. 3c and d) that could be compensated for by adjusting the reservoir size.

To accommodate the large volumes in the reagent reservoirs without significantly increasing device footprint, we placed a cleanroom wipe made of paper (Durx 670, Berkshire Corporation, USA) atop the capillary pump.[33] The combination of 3D-printing and off-the-shelf, low cost paper saves costs without compromising performance. The driving capillary pressure in the circuit is defined by capillary pump because the gap between the edge of the PDMS and the paper forms an open microchannel that can be drained. Hence, the capillary pressure is dictated by the capillary pressure of the capillary pump, allowing use of paper pumps with higher, but sometimes ill-defined capillary pressures, without impacting the accuracy and functionality of the CCs.

Requirements for sequential RBV bursting. It is not sufficient to simply increase the burst pressure of the RBV to achieve sequential drainage and in fact the architecture of the CC must be designed to ensure that an RBV only bursts after complete drainage of the reservoir connected to the previous RBV. To illustrate this point, the proof of concept CC shown in Fig. 3a when filled with liquid is modeled by an electrical equivalent circuit shown in Fig. 4a.

Considering the circuit at the instant when all reservoirs are filled, but still under static conditions, without flow, the junction pressure P_J will be equal to the pressure P_C of the capillary pump. Given that the capillary pressure of the pump is larger than the capillary pressure of the side branches, liquid will be drawn towards the junction P_J, leading to flow in the CC. The first side branch to be drained in the CC is the one connected to the RBV with the lowest burst pressure, which here is RBV1 with pressure P_1. As liquid drains from side branch 1, there is a pressure drop across R_1 and R_{RV} on one hand and across the main resistor R_M on the other hand, which will lead to a reduction of the pressure P_J at the juncture between the side-branch and the main channel. The high resistance of R_{RV} and R_M compared to the low resistance of the release channel ensures that pressure P_J is replicated

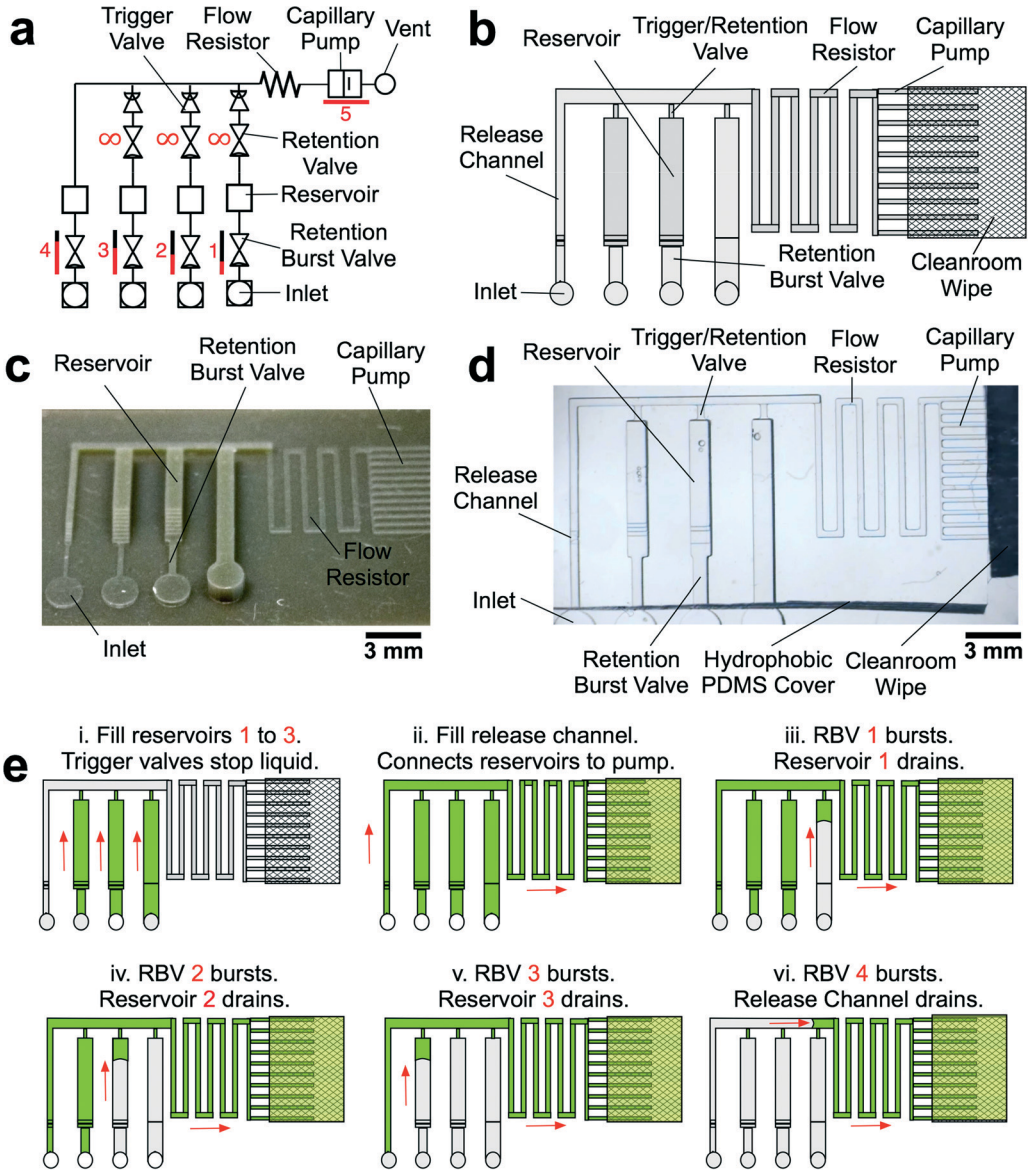

Fig. 3 Design, mold, PDMS replica and operation of CCs for autonomous sequential delivery of four liquids. a) Symbolic representation of CC with main fluidic elements labelled. b) Schematic of CC. c) 3D-printed mold of the CC and d) PDMS replica with transparent PDMS cover and clean room wipe contacting the capillary pump. e) Schematic illustrating expected operation of RBVs. Solutions loaded into the reservoirs are delivered in pre-programmed manner according to RBV capillary pressure.

across all 4 junctions (red dot in Fig. 4a). To avoid bursting of RBV2 while branch 1 is draining, it is imperative that $|P_J| < |P_2|$ at all times. Assuming a single branch drains at any given time, the pressure P_J during drainage of the RBV can be calculated from the electrical circuit analogue using Kirchhoff's law and Ohm's law yielding:

$$P_J = \frac{P_i R_M + P_c (R_{RV} + R_i)}{(R_M + R_{RV} + R_i)} \quad (3)$$

where the index i represents the side branch that is being drained in the capillary circuit, P_i is the capillary pressure of the liquid meniscus on the end of the side branch, R_i is the flow resistance of the RBV and reservoir of the side branch, R_{RV} is the resistance of the retention valve, R_M is the flow resistance of the main resistor, and P_c is the pressure of the capillary pump (see Fig. 4a).

As the liquid drains, the resistance in the side branch is expected to change. However, the retention/trigger valve structure has the smallest cross-section ($300 \times 50\ \mu m^2$) in the side branch and its associated resistance $R_{RV} > 100R_i$. Consequently, changes in the resistance of the side branch during drainage are negligible and do not need to be considered in the calculation of P_J. Moreover, after the RBV drains, P_J decreases since the capillary pressure at the end of the side branch now becomes the capillary pressure of the reservoir rather than the capillary pressure of the RBV. This drop in P_J does not adversely affect sequential liquid delivery since the condition for sequential liquid delivery is still met; in fact,

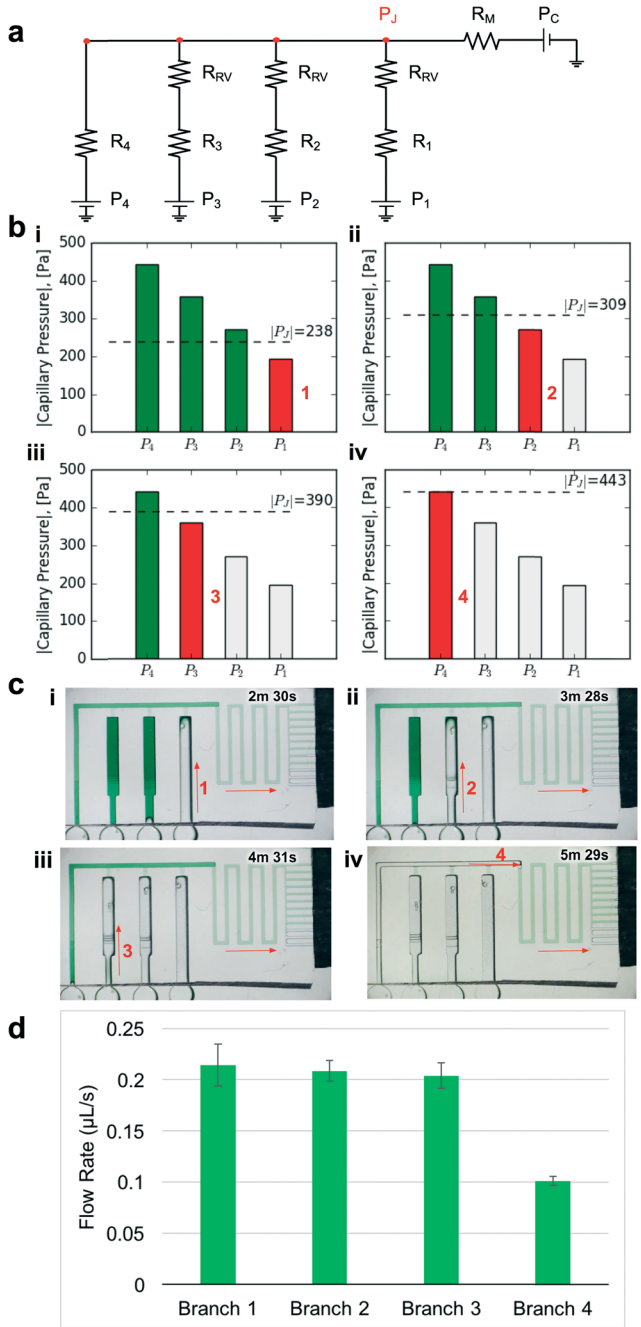

Fig. 4 Design and experimental validation of CC for autonomous delivery of four liquids. a) Electric circuit analogue showing the flow resistances and capillary pressures in the CC. b) Graphs showing the calculated junction pressures during bursting of each RBV. Junction pressures were designed to ensure that RBVs burst sequentially. c) Time-lapse images showing autonomous and sequential drainage of reservoirs in the CC. Arrows represent sequence and flow direction. Text labels show time during liquid delivery. A video of the autonomous liquid delivery operation is provided in movie S1.† d) Flow rates for different branches of the capillaric circuit. N = 3 devices from different 3D-printed molds. Error bars represent standard deviation.

during reservoir drainage one expects liquid delivery to be even more sequential since the junction pressure is lower. Hence the most stringent condition on P_J is given by the situation described by the electrical circuit with fully filled conduits, which can thus be used to establish the conditions for sequential drainage of each of the side branches.

The required condition for junction pressure to ensure that only one RBV in the CC bursts can be generalized as follows:

$$P_J < P_{i+1} \quad \text{during drainage of branch } i \tag{4}$$

where P_{i+1} is the capillary pressure of the next RBV to burst in the circuit. This condition can be satisfied by balancing the flow resistance in the circuit, and in particular adjusting the main flow resistance (R_M) in front of the capillary pump to ensure that P_J during drainage is lower than the pressure of the subsequent RBVs (see Fig. 4a). This calculation is applicable to CCs where the resistance of the channel linking the side branches is negligible compared to R_{RV}, or else that resistance must also be considered and the appropriate analogous electrical model derived and resolved. The calculation holds for the model CC and can be used to calculate the pressure P_J during drainage of branch i and ensure that it is smaller than the retention pressure P_{i+1} of branch i + 1 (Fig. 4b).

The geometries of the RBVs in the CC are summarized in Table 1. We designed our proof-of-principle device to obtain uniform capillary pressure differences of 80 ± 5 Pa between successive valves. All RBVs were 2.6 mm long. We designed a 4.2 mm long, 290 μm wide, and 100 μm deep main resistor so that the junction pressure during each liquid delivery step satisfied our condition for sequential liquid delivery (see Fig. 4b).

Contact angle hysteresis must be taken into account when designing the capillary pump to ensure that the capillary pressure threshold for all RBVs can be overcome. Since the filling of the capillary pump is dictated by the advancing contact angles on the microchannel walls while the bursting of the RBVs is dictated by the receding contact angles on the microchannel walls, the dimensions of the capillary pump must be significantly smaller than the smallest dimension of RBVs to ensure drainage.[13] Thus, the capillary pump in our proof-of-principle 4-valve circuit was using microchannels that were 200 × 100 μm^2, providing a wicking capillary pressure of −736 Pa that is large enough to drain each RBV in the circuit.

To experimentally validate our design, we 3D-printed the CC mold with our calculated dimensions for the main resistor and made PDMS replicas as described earlier (see Fig. 3).

Table 1 Geometry of retention burst valves (RBVs) for autonomous delivery of four liquids. Junction pressures during drainage of RBVs were calculated using eqn (3)

	RBV1	RBV2	RBV3	RBV4
Width (μm)	960	670	480	380
Height (μm)	1000	750	650	550
RBV pressure P_i (Pa)	−194	−271	−358	−441
P_J during drainage (Pa)	−238	−309	−390	−443

Then we tested liquid delivery using aqueous food dye solutions. As expected, each side branch drained sequentially without drainage of the other RBVs (Fig. 4c and movie S1†). Pre-programmed drainage of the side branches was completed within 4 min. The sequence of RBV drainage was 100% successful over four repeated tests with devices made from three different 3D-printed molds. As shown in Fig. 4d, the flow rates for liquid drainage from branches 1, 2, 3, and 4 were 0.21 ± 0.02, 0.21 ± 0.01, 0.20 ± 0.01, and 0.10 ± 0.01 μL s^{-1} respectively. Next we tested whether reproducibility of flow rate could be further improved by using three replicates from a single mold, but the variability remained comparable, suggesting that user manipulations and other parameters, but not the 3D-printer imprecision, are the main source of variability.

Capillaric circuit for autonomous delivery of eight liquids. After establishing general guidelines for designing RBVs to obtain sequential liquid delivery, we designed a CC with eight liquid delivery steps, double the number in our proof-of-principle CC and exceeding the number of sequentially-encoded, self-regulated microfluidic drainage events in our previous work with cleanroom-fabricated CCs.[13]

As described earlier, the smallest microchannel width that we could print without a high incidence of defects was 200 μm. We designed the capillary pump region of the CC to be 300 μm wide and 50 μm deep to ensure reliable printing since the capillary pump has a larger pressure than all the RBVs in the circuit. To encode capillary pressure differences, we systematically varied the heights and widths of microchannels in each side branch (see Table 2). We designed RBVs according to the junction pressure criterion (see eqn (4)) to ensure that valves were drained sequentially. Although in theory, very small differences in capillary pressure between successive RBVs should ensure serial drainage, empirical tests yield that designed capillary pressure differences of ~40 Pa provided reliable sequential drainage of RBVs. This empirical value depends on the resolution and accuracy of features produced by the 3D printer and might be reduced with a more accurate printer, or conversely might need to be increased for experiments that require solutions with different surface tensions that will affect the contact angle and the capillary pressure P_i of the RBV and branch loaded with this solution.

The main resistor was 18.5 mm long, 300 μm wide, and 50 μm deep to obtain a calculated drainage time of ~10 min for all 8 liquid delivery steps based on the capillary pressures, resistances, and volumes of the microchannels in the circuit. The smallest RBV in the circuit was 380 μm wide and 200 μm deep. Since this valve was much shallower than the reservoir (960 μm wide and 1000 μm deep), we connected the valve to the reservoir using a gently sloped staircase with 50 μm height increments to prevent from liquid stopping due to the formation of an undesired stop valve. We set the maximum channel height in our CCs to 1 mm to stay within a regime where capillary forces are dominant. These geometric constraints limited the number of RBVs, and by extension the number of liquid delivery steps that we could automate in our CCs.

We experimentally validated the operation of the 8-step circuit by 3D-printing a mold and making PDMS replicas as described previously. Fig. 5 shows time-lapse images of autonomous and sequential delivery of 8 liquids in the CC. The autonomous sequential liquid delivery is shown in movie S2.† Liquids were initially pre-loaded into the reagent reservoirs, and then the central release channel was filled with 10 μL of liquid to start the autonomous drainage operations. Following drainage of the solution from inlet 8 and pinning of the air–liquid interface at RBV8 in the trigger channel, RBV1 is the first to start bursting at t = 3 min 11 s. Each RBV with its attendant reservoir take ~50 s to drain and the autonomous drainage of the 8 solutions was completed in <7 min.

Comparison between 3D-printed and cleanroom-fabricated capillaric circuits. Cleanroom fabrication allows microchannel height and width specifications down to 1 μm and less, whereas with the 3D printer used here the resolution was limited ~200 μm in XY and 50 μm in Z. Consequently, one can more finely vary the capillary pressures of microfabricated CCs, which in theory could allow sequential drainage of more channels. However, sequential drainage is constrained by the whole circuit architecture to ensure that the condition for sequential drainage of all the retention burst valves in the capillary circuit is still met (eqn (3) and (4) and Fig. 4a).

A strength of 3D printing is the capability to print multi-height features in a single run, whereas when using classical photolithography each different depth level would require a photolithographic and processing step with precise alignment which would make fabrication excessively slow, costly and at the same time reduce the yield. For example, the CC for the autonomous delivery of eight liquids used seven different depths on the same mold (see Fig. 5).

Capillary forces are dominant over gravitational and inertial forces at the scale of the conduits used for the CCs shown here. However, the 3D-printed conduits extend over several tens of millimetres in some cases, and if a chip is not horizontal, or in the most extreme case if it is positioned

Table 2 RBVs designed for autonomous delivery of eight liquids

	RBV1	RBV2	RBV3	RBV4	RBV5	RBV6	RBV7	RBV8
Width (μm)	770	670	580	480	380	380	380	380
Height (μm)	900	750	650	600	600	400	300	200
Valve pressure P_i (Pa)	−233	−270	−314	−365	−430	−483	−536	−642
P_J during drainage (Pa)	−250	−286	−329	−379	−442	−493	−544	−643

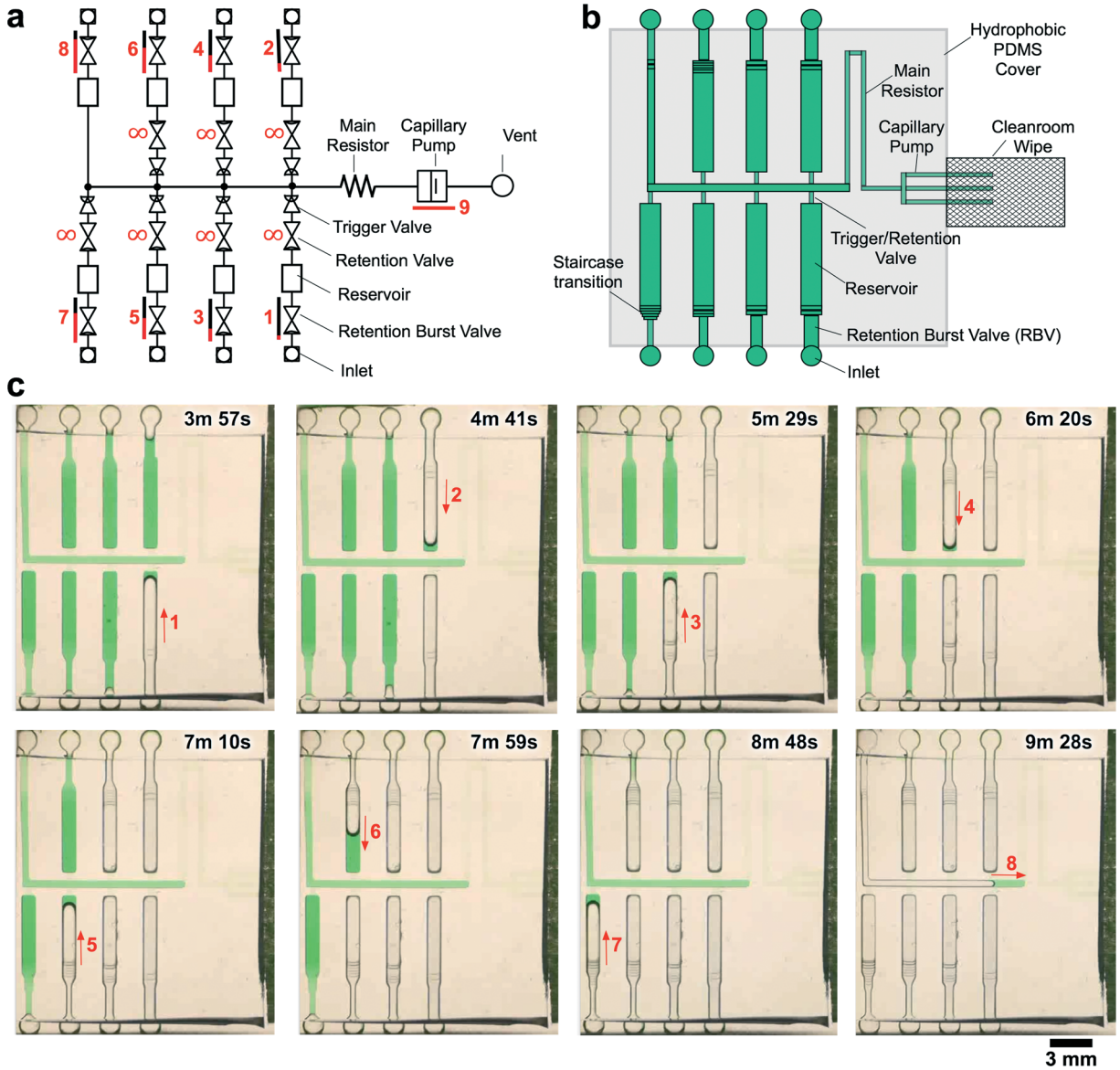

Fig. 5 CC for autonomous delivery of eight liquids. a) Symbolic representation of CC showing modular assembly of fluidic elements. b) Schematic representation of CC. c) Time-lapse images showing autonomous delivery of 8 liquids in the CC. Arrows indicate flow direction and numbers highlight the time and sequence of liquid delivery. A video of liquid delivery is provided in movie S2.†

Table 3 Summary of calculated and empirical design rules for CCs with TVs and RBVs printed using the EnvisionTEC MicroEDU 3D-printer, and replicated into PDMS with surface properties described in the text and under the condition that all solutions have the same surface tension

Design rules for capillaric circuits made from 3D-printed molds	
Maximal conduit size to stay within capillary microfluidic regime: Channel width: $w \leq 1$ mm Channel height: $h \leq 1$ mm	Minimal feature size imposed by EnvisionTEC MicroEDU 3D-printer: Channel width: $w > 200$ um Channel height: $h \geq 50$ μm Max. device footprint: 75 × 100 mm^2 Min. step between two widths: $\Delta w = 100$ μm Min. step between two heights: $\Delta h = 50$ μm
Trigger valve (TV) design rules: 1. Height difference between TV and release channel: $\Delta h \geq 300$ μm	Retention burst valve (RBV) design rules: 1. Difference in capillary pressure between successive RBVs: $\Delta P > 40$ Pa 2. Condition for sequential delivery of liquids in CC with side branches with high-resistance retention valves connected to a main channel with pressure P_J: $\lvert P_J \rvert < \lvert P_{i+1} \rvert$ during drainage of branch i

such that the channel is vertical, then the hydrostatic pressure could disrupt the functionality of the CC and notably the pre-programmed drainage order. For the 8-valve CC the difference between two sequential retention burst valves is 40 Pa, which corresponds to the pressure of a water column height of 4 mm. The footprint of the 8-valve CC is much larger, and by placing it on one of the sides at a 90° tilt, the sequence of drainage was disrupted, as predicted. Hence, for the reliable operation of CCs with large conduits and incremental differences in capillary pressure it is important to consider the position of the CC, and ideally to position the devices horizontally.

Conclusions

Taken together, our results indicate that 3D-printing allows rapid and inexpensive fabrication of reliable capillaric valves and circuits.

We established design rules for CCs, TVs, and RBVs (see Table 3). These design rules are specific to our 3D-printer and the PDMS replicas with a hydrophobic top surface (advancing and receding contact angles of 114° and 89°, respectively) and hydrophilic bottom and side surfaces (advancing and receding contact angles 45° and 31°, respectively). The resolution reliably achievable with the consumer grade 3D printer used here was limited to ~200 μm. The design of a CC must consider multiple, sometimes competing, conditions for achieving the desired number of sequential events, flow rates, and time of delivery. With further improvements and better 3D-printers and resolution, higher capillary pressures could be generated, and more RBVs and liquid delivery steps could be included in the CC, thus increasing the possibilities of CCs.

The skill and resources needed to make CCs from 3D-printed molds lies between paper microfluidics and cleanroom-fabricated capillary microfluidics. The replication step into PDMS that was used here only adds a few hours to the iteration time. Whereas direct printing is desirable, a replication step also has benefits as the mold of the best working CC is preserved, and could serve as a master mold for subsequent mass production of CCs by hot embossing or injection molding.

With the widespread adoption of 3D-printers, CCs could be readily printed by many researchers, and the design rules presented here will facilitate the fabrication of functional circuits. 3D-printing of CCs is especially appealing as a way to rapidly iterate through multiple designs and test new functions. In the future, it would be desirable to replace PDMS – which only retains its hydrophilicity for a few hours after plasma treatment[34] – with alternate polymers with more stable hydrophilic surfaces,[35] either by directly 3D printing them, or by replication into stable polymers. 3D-printed autonomous CCs may be developed for large-volume and multi-step biochemical assays to be used for point-of-care diagnosis, for research in a lab, as well as for educational purposes.

Acknowledgements

We acknowledge NSERC and CIHR for funding. A. O. acknowledges financial support from the NSERC CREATE Integrated Sensor Systems Training Program, the CIHR Systems Biology Training Program, and an FRQNT PBEEE Scholarship. D. J. acknowledges a Canada Research Chair. We acknowledge support from the McGill Nanotools Microfab. We thank Nicolas Broduch and Professor Raynald Gauvin in the Department of Materials Engineering at McGill University for Scanning Electron Microscopy support. A. O. also acknowledges helpful discussions with Arya Tavakoli, Donald MacNearney, Jeffrey Munzar, and Philippe DeCorwin-Martin at McGill University, Steven Jim at the University of California, Irvine, and writing feedback from members of his McGill Graphos Peer Writing Group.

References

1 P. F. Man, C. H. Mastrangelo, M. A. Burns and D. T. Burke, *Proceedings of the IEEE Micro Electro Mechanical Systems (MEMS)*, Heidelberg, Germany, 1998.
2 D. Juncker, H. Schmid, U. Drechsler, H. Wolf, M. Wolf, B. Michel, N. de Rooij and E. Delamarche, *Anal. Chem.*, 2002, **74**, 6139–6144.
3 J. Melin, N. Roxhed, G. Gimenez, P. Griss, W. Vanderwijngaart and G. Stemme, *Sens. Actuators, B*, 2004, **100**, 463–468.
4 R. Safavieh, A. Tamayol and D. Juncker, *Microfluid. Nanofluid.*, 2014, **18**, 357–366.
5 M. Zimmermann, H. Schmid, P. Hunziker and E. Delamarche, *Lab Chip*, 2007, **7**, 119–125.
6 L. Gervais, M. Hitzbleck and E. Delamarche, *Biosens. Bioelectron.*, 2011, **27**, 64–70.
7 L. Gervais and E. Delamarche, *Lab Chip*, 2009, **9**, 3330–3337.
8 M. Zimmermann, P. Hunziker and E. Delamarche, *Biomed. Microdevices*, 2008, **11**, 145–163.
9 E. Fu, S. A. Ramsey, P. Kauffman, B. Lutz and P. Yager, *Microfluid. Nanofluid.*, 2010, **10**, 29–35.
10 X. Li, D. R. Ballerini and W. Shen, *Biomicrofluidics*, 2012, **6**, 11301–1130113.
11 P. Novo, F. Volpetti, V. Chu and J. P. Conde, *Lab Chip*, 2013, **13**, 641–645.
12 S. J. Kim, S. Paczesny, S. Takayama and K. Kurabayashi, *Lab Chip*, 2013, **13**, 2091–2098.
13 R. Safavieh and D. Juncker, *Lab Chip*, 2013, **13**, 4180–4189.
14 J. Berthier, D. Gosselin and E. Berthier, *Microfluid. Nanofluid.*, 2015, **19**, 497–507.
15 M. I. Mohammed and M. P. Y. Desmulliez, *Microsyst. Technol.*, 2013, 1–10.
16 A. Kazemzadeh, P. Ganesan, F. Ibrahim, S. He and M. J. Madou, *PLoS One*, 2013, **8**(9), e73002.
17 K. Ellinas, A. Tserepi and E. Gogolides, *Microfluid. Nanofluid.*, 2014, **17**, 489–498.
18 K. Kistrup, C. E. Poulsen, P. F. Østergaard, K. B. Haugshøj, R. Taboryski, A. Wolff and M. F. Hansen, *J. Micromech. Microeng.*, 2014, **24**, 125007.

19 J. L. Moore, A. McCuiston, I. Mittendorf, R. Ottway and R. D. Johnson, *Microfluid. Nanofluid.*, 2010, **10**, 877–888.
20 A. K. Au, W. Huynh, L. F. Horowitz and A. Folch, *Angew. Chem., Int. Ed.*, 2016, **55**, 3862–3881.
21 B. C. Gross, J. L. Erkal, S. Y. Lockwood, C. Chen and D. M. Spence, *Anal. Chem.*, 2014, **86**, 3240–3253.
22 A. I. Shallan, P. Smejkal, M. Corban, R. M. Guijt and M. C. Breadmore, *Anal. Chem.*, 2014, **86**, 3124–3130.
23 A. K. Au, W. Lee and A. Folch, *Lab Chip*, 2014, **14**, 1294–1301.
24 D. J. Guckenberger, T. E. de Groot, A. M. D. Wan, D. J. Beebe and E. W. K. Young, *Lab Chip*, 2015, **15**, 2364–2378.
25 D. Qin, Y. Xia and G. M. Whitesides, *Nat. Protoc.*, 2010, **5**, 491–502.
26 M. Pla-Roca and D. Juncker, in *Methods in Molecular Biology*, ed. A. Khademhosseini, K.-Y. Suh and M. Zourob, Humana Press, Totowa, NJ, 2010, vol. 671, pp. 177–194.
27 H. Bruus, *Theoretical microfluidics*, OUP Oxford, 2008.
28 M. Zimmermann, P. Hunziker and E. Delamarche, *Microfluid. Nanofluid.*, 2008, **5**, 395–402.
29 A. Glière and C. Delattre, *Sens. Actuators, A*, 2006, **130-131**, 601–608.
30 M. I. Mohammed, E. Abraham and M. P. Y. Desmulliez, *J. Micromech. Microeng.*, 2013, **23**, 035034.
31 S. Cesaro-Tadic, G. Dernick, D. Juncker, G. Buurman, H. Kropshofer, B. Michel, C. Fattinger and E. Delamarche, *Lab Chip*, 2004, **4**, 563–569.
32 S. Bergeron, V. Laforte, P.-S. Lo, H. Li and D. Juncker, *Anal. Bioanal. Chem.*, 2015, **407**, 8451–8462.
33 M. Wolf, D. Juncker, B. Michel, P. Hunziker and E. Delamarche, *Biosens. Bioelectron.*, 2004, **19**, 1193–1202.
34 D. Bodas and C. Khan-Malek, *Sens. Actuators, B*, 2007, **123**, 368–373.
35 C. F. Carlborg, T. Haraldsson, K. Öberg, M. Malkoch and W. van der Wijngaart, *Lab Chip*, 2011, **11**, 3136–3147.